Environmental and Climate Technologies
2025, vol. 29, no. 1, pp. 552–561
https://doi.org/10.2478/rtuect-2025-0038
https://content.sciendo.com

Thermal Performance Analysis of Phase Change Material Based Thermal Energy Storage

Saulius PAKALKA[1]*, Jolanta DONĖLIENĖ[2], Tomas RAZVANOVIČIUS[3]

[1,2]*Applied Research Institute for Prospective Technologies, Vismaliuku str. 34, 10243, Vilnius, Lithuania*
[1–3]*Modernios E-Technologijos, UAB, Vismaliuku str. 34, 10243 Vilnius, Lithuania*

Received 19.03.2025; accepted 26.08.2025

***Abstract* – The study presents an experimental analysis of the thermal performance of a high energy density phase change material (PCM)-based thermal energy storage (TES) prototype (PCM TES). The PCM TES is designed for use in heating and domestic hot water preparation systems within a temperature range of 40–60 °C. Charging and discharging experiments were conducted using an experimental setup, and several parameters were analysed, including heat transfer fluid (HTF) temperature and mass flow rate, PCM temperature, PCM charging and discharging time, heat transfer rate of the heat exchanger, and stored and released thermal energy. The experiment showed that during the charging process, at a mass flow rate of 0.1 kg/s and an average inlet temperature of hot water of 72 °C, the heat transfer rate decreased from 20.9 kW to 3.4 kW, with an average of 9.3 kW. During the discharging process, at a mass flow rate of 0.1 kg/s and an average cold water inlet temperature of 16 °C, the heat transfer rate decreased from 19.2 kW to 2.2 kW, with an average of 10.6 kW. The amount of heat absorbed and released in the PCM temperature range of 20–70 °C was 7.48 kWh, and the duration of the charging and discharging was 48 min and 37 min 49 s, respectively.**

***Keywords* – Domestic Hot Water (DHW); heat exchanger; latent heat; Phase Change Material (PCM).**

Nomenclature

c_p	Specific heat capacity at constant pressure	J/kgK
$\dot{m}$	Mass flow rate	kg/s
$\dot{Q}$	Heat transfer rate	kW
Q	Energy	kWh
T	Temperature	°C
τ	Time	s
Abbreviations		
C	Cooler	–
DHW	Domestic hot water	–
EMV	Electronic mixing valve	–
EV	Expansion vessel	–
H	Heater	–

* Corresponding author.
E-mail address: s.pakalka@protechnology.lt

©2025 Author(s). This is an open access article licensed under the Creative Commons Attribution License (http://creativecommons.org/licenses/by/4.0).

HTF	Heat transfer fluid	–
HX	Heat exchanger	–
L	Loop	–
F	Flow meter	–
PCM	Phase change material	–
PCM TES	Phase change material-based thermal energy storage	–
P	Pump	–
ST	Storage tank	–
TES	Thermal energy storage	–
V	Valve	–
Subscripts		
1, 2, 3	Position number	
AVE	Average	

1. INTRODUCTION

Latent heat thermal energy storage (TES) plays an important role in increasing the energy density of storage systems. Phase change materials (PCMs) are increasingly used as a latent heat storage medium. However, due to the low thermal conductivity of most PCMs, ensuring effective heat transfer between heat transfer fluid (HTF) and PCM is crucial. High PCM charging and discharging rates contribute to the efficient use of renewable energy sources in heating and domestic hot water (DHW) systems. The implementation of PCM-based TES includes various applications, such as heat pumps [1], [2], solar DHW systems [3]–[5], power-to-heat systems that use electricity from photovoltaic modules or power grid [6], [7], district heating [8], and building envelopes [9], [10].

Different heat transfer enhancement methods are analysed to improve the charging and discharging rates of PCM TES and achieve high energy density. One design concept to overcome the low thermal conductivity of PCM involves using a heat exchanger (HX) with a large heat transfer surface area. The development of HX includes numerical and experimental investigations [11], testing thermal performance under different operating conditions [12], and implementing thermal enhancement techniques [13], [14].

Fadl *et al.* [15] conducted an experimental analysis of the thermal performance of a compact latent heat storage prototype containing a horizontally oriented shell-and-tube heat exchanger. The influence of different operating conditions, including the heat transfer fluid (HTF) volume flow rate and inlet temperature, on power input and output, melting and solidification time, and the energy stored and released was evaluated during the charging and discharging stages. Muraleedharan Nair *et al.* [16] analysed the thermal performance of PCM-based shell-and-tube heat exchangers for domestic hot water applications. Different HX geometries and heat transfer enhancement techniques were experimentally investigated, including longitudinal and circular fins, as well as expanded graphite (EG). Thonon *et al.* [17] presented a review of HX operating under a simultaneous charging-discharging process. Recommendations were suggested for performance evaluation, PCM selection, and the geometry of the storage and the heat exchangers. Herbinger & Groulx [18] performed experimental characterization of a finned-tube PCM heat exchanger with three different numbers of vertical-finned tubes. They tested different operating conditions and geometrical

arrangements by performing PCM charging and discharging using both parallel and series flow configurations. It was found that heat transfer rates were slightly lower in series configuration due to the continuously decreasing temperature of HTF.

The aim of this study is to analyse the thermal performance of novel PCM TES prototype, the design of which is based on the external arrangement of PCM and two-loop heat exchanger. To utilise maximum heat transfer surface area of the HX both loops are connected in series configuration. This experiment evaluates thermal performance during PCM TES charging and discharging cycles. The HTF and PCM temperature, PCM charging and discharging time, the heat transfer rate of the heat exchanger, and stored and released thermal energy are monitored and analysed.

2. EXPERIMENTAL SETUP AND METHODOLOGY

The object of this study is a full-scale PCM-based TES unit (PCM TES) designed for use in heating and domestic hot water (DHW) preparation systems within a temperature range of 40–60 °C. The PCM TES prototype consists of a thermally insulated storage tank, a compact two-loop (L1 and L2) fin-and-tube type heat exchanger (Fig. 1), and an organic PCM RT58 (manufacturer Rubitherm). The parameters of the PCM TES unit and the thermophysical properties of PCM RT58 are presented in Table 1.

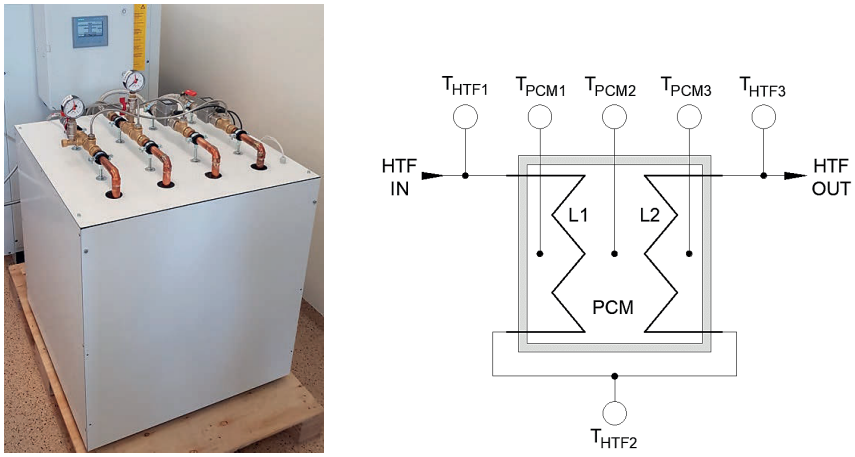

Fig. 1. General view and schematic representation of the PCM TES.

The PCM TES charging and discharging experiments were performed using an experimental setup consisting of buffer tanks with an electric heater and cooler for the preparation of hot and cold HTF (water), a mixing valve with an actuator and an electronic constant temperature controller, flow meters, circulating pumps, expansion vessels, six temperature sensors (Pt100), process control and monitoring system. A schematic representation of the experimental setup is shown in Fig. 2.

TABLE 1. PARAMETERS OF ANALYSED PCM TES AND PCM RT58

PCM TES		**Properties of PCM RT58**	
External dimensions (H/W/D), mm	740/720/720	Heat storage capacity (combination of latent and sensible heat in a temperature range of 50–65 °C), kJ/kg	160±7.5 %
Fin quantity, units	70	Melting area, °C	53–59
Fin spacing, mm	5	Congealing area, °C	59–53
Fin thickness, mm	0.15	Specific heat capacity, kJ/kgK	2.0
Tube diameter (OD), mm	12.7	Density solid, kg/L	0.88
Tube thickness, mm	0.5	Density liquid, kg/L	0.77
Heat exchanger weight, kg	32.6	Thermal conductivity (both phases), W/mK	0.2
HX heat transfer area, m^2	33.8	Volume expansion, %	12.5
PCM mass, kg	93	Max operation temperature, °C	80

Fig. 2 shows the schematic drawing of the experimental setup, which consists of PCM TES, PCM temperature sensors $T_{PCM1\ –\ PCM3}$, HTF temperature sensors $T_{HTF1\ –\ HTF3}$, tanks for hot and cold water storage (ST1, ST2), expansion vessels (EV1, EV2), water heater (H), water cooler (C), mixing valve with electronic constant temperature controller (EMV), manual valves (V1.1, V1.2, V2.1, V2.2), flow meters (F1, F2) and circulating pumps (P1, P2). The experimental setup is described in more detail in [19], [20].

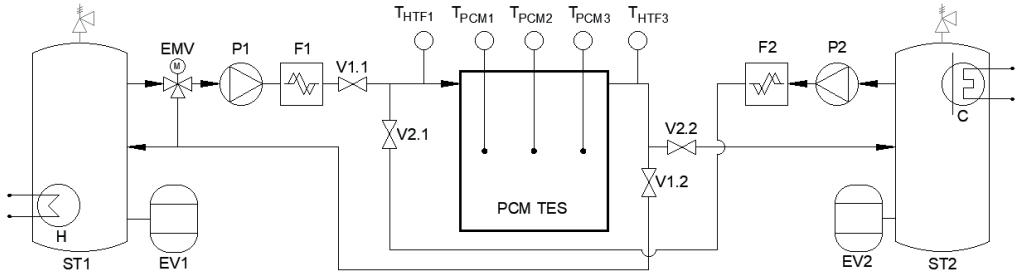

Fig. 2. Schematic representation of the experimental setup.

Experiments are carried out using a constant HTF (water) mass flow rate of 0.1 kg/s, which is selected based on eco-design requirements for water heaters [21]. At the beginning of the charging (melting) process, the PCM is in the solid phase at an average temperature of 20 °C. Hot HTF at the average temperature of 72 °C is supplied to HX of PCM TES by opening valves V1.1 and V1.2. The end of the charging process is determined by the average temperature of the PCM, and it is stopped when it reaches 70.0 °C. At this temperature, the PCM is in the liquid phase, and the discharging process is then initiated. Cold HTF at an average temperature of 16 °C is supplied to HX of the PCM TES by opening valves V2.1 and V2.2. The discharging process is complete when the average temperature of the PCM returns to the initial temperature of 20.0 °C, ensuring that both the charging and discharging processes begin and end with the same initial conditions and reference temperatures (70.0 °C and 20.0 °C).

The PCM TES is insulated with 50 mm thick polyurethane thermal insulation, with a thermal conductivity of 0.022 W/mK. Based on the standard [22], it was calculated that the

average heat loss was 42 W. Considering the amount of energy stored during the charging experiment, the heat loss accounts for 0.55 %. It is therefore assumed that average heat loss is low and does not significantly influence test results.

The main parameters measured were the mass flow rate and the temperature. The data logging interval for the charging and discharging process is 1 s. The temperature was measured using Pt100 temperature sensors (class B, accuracy ± (0.3 + 0.005 × T) °C). The water mass flow rate was measured with a mass flow meter (accuracy ± 0.15 % of the actual measured flow rate). Based on Eq. (1), the uncertainty in the heat transfer rate was determined to be ±1.53 %.

$$\frac{\Delta\dot{Q}}{\dot{Q}} = \sqrt{\left(\frac{\Delta\dot{m}}{\dot{m}}\right)^2 + \left(\frac{\Delta x}{x}\right)^2}\,, \tag{1}$$

where $\Delta\dot{Q}/\dot{Q}$ – relative error of heat transfer rate; $\Delta\dot{m}$ – mass flow rate absolute error; $\dot{m}$ – measured mass flow rate of HTF; $\Delta x = \sqrt{\left(\Delta T_1\right)^2 + \left(\Delta T_2\right)^2}$, and $x = T_1 - T_2$, T_1 and T_2 are the temperatures at the beginning and at the end of the process; ΔT_1 and ΔT_2 – absolute error of temperature sensors respectively.

The heat transfer rate $\dot{Q}$ between the HTF (water) and the PCM was obtained by the following Eq. (2):

$$\dot{Q} = \dot{m} \cdot c_{\mathrm{p}} \cdot \mathrm{d}T\,, \tag{2}$$

where $\dot{m}$ is the mass flow rate of the heat transfer fluid, kg/s; c_{p} is the specific heat capacity at constant pressure, J/kgK; dT is the temperature difference, K.

The amount of heat Q transferred during time interval $\Delta\tau$ is calculated by using Eq. (3).

$$Q = \dot{Q} \cdot \frac{\Delta\tau}{3600} \tag{3}$$

The time interval $\Delta\tau$ in this experiment is 1 s. The heat transfer rate during each 1 s interval is constant. The total amount of heat is the sum of the heat transferred during each time interval.

3. Results and Discussion

The thermal performance of PCM TES is analysed during the charging and discharging cycles. This includes monitoring the HTF (water) and PCM temperature, the HTF mass flow rate, and evaluation of the heat transfer rate and energy. The average temperature of PCM ($T_{\mathrm{PCM,\,AVE}}$) is calculated based on the three temperature sensors located in the PCM (T_{PCM1}, T_{PCM2}, and T_{PCM3}).

3.1. PCM TES Charging

The PCM TES charging (PCM melting) experiment showed the temperature variations of the HTF and PCM, the heat transfer rate of the HX, and the amount of absorbed heat. The temperature distribution graph is presented in Fig. 3, and the heat transfer rate and energy curves for the entire charging process are shown in Fig. 4.

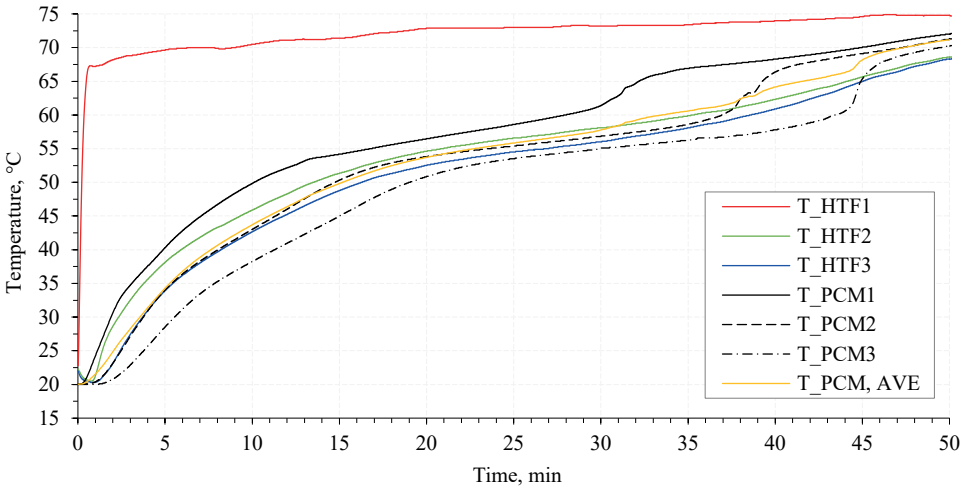

Fig. 3. Temperature distribution of HTF and PCM during the charging (melting) process.

Fig. 3 shows a large temperature difference (ΔT) between the inlet (T_{HTF1}) and outlet (T_{HTF2}) HTF of the first loop L1. In this case, ΔT decreases from 46.4 °C at the beginning of the charging process to 7.1 °C at the end, with an average ΔT of 18.7 °C. The temperature difference between the inlet (T_{HTF2}) and outlet (T_{HTF3}) HTF of the second loop L2 is significantly lower compared to L1, reaching a maximum ΔT of 5.6 °C after 2 minutes from the beginning of the process. The average ΔT of L2 during the entire process is 2.2 °C. This indicates that the heat transfer rate of L1 is significantly higher than that of L2. The temperature of PCM increases more rapidly at the measurement point T_{PCM1}, located closest to the inlet manifold of HX.

A similar temperature profile is observed for measuring points T_{PCM2} and T_{PCM3}, but with a temperature difference between them. The highest ΔT between T_{PCM1} and T_{PCM2} is 8.4 °C at 34 min 30 s, and between T_{PCM2} and T_{PCM3} is 9.1 °C at 41 min 18 s. The temperature of the PCM at T_{PCM1} reaches a melting point of 53 °C after 12 min 48 s from the start of the experiment, at T_{PCM2} after 18 min 7 s, and at T_{PCM3} after 23 min 28 s. From Fig. 3, it can be observed that once the temperature surpasses 53 °C, the incline of the temperature curves diminishes. This indicates phase transition from solid to liquid and storage of latent heat. The temperature of the PCM at T_{PCM1} reaches the upper range of the phase transition 59 °C after 25 min 48 s from the start of the experiment, at T_{PCM2} after 35 min 35 s, and at T_{PCM3} after 42 min 12 s. This means that the PCM is in the liquid phase, and the slope of the temperature curves increases, indicating sensible heat transfer. The duration of the charging process, until the average PCM temperature reaches 70 °C, is 48 minutes.

The heat transfer rate during the charging process varies depending on the temperature difference between HTF and PCM, see Fig. 4.

Fig. 4 shows that the heat transfer rate reaches a maximum value of 20.9 kW at 48 s from the beginning of charging and decreases to 3.4 kW when the average PCM temperature ($T_{PCM, AVE}$) reaches 70 °C (48 min). The average heat transfer rate during the entire charging process is 9.3 kW. The amount of heat absorbed, in the average PCM temperature range of 20–70 °C, is 7.48 kWh. Due to the higher heat transfer rate at the beginning of the process, 42.8 % or 3.2 kWh of heat is stored until the PCM temperature (T_{PCM1}) reaches a melting point at 12 min 48 s.

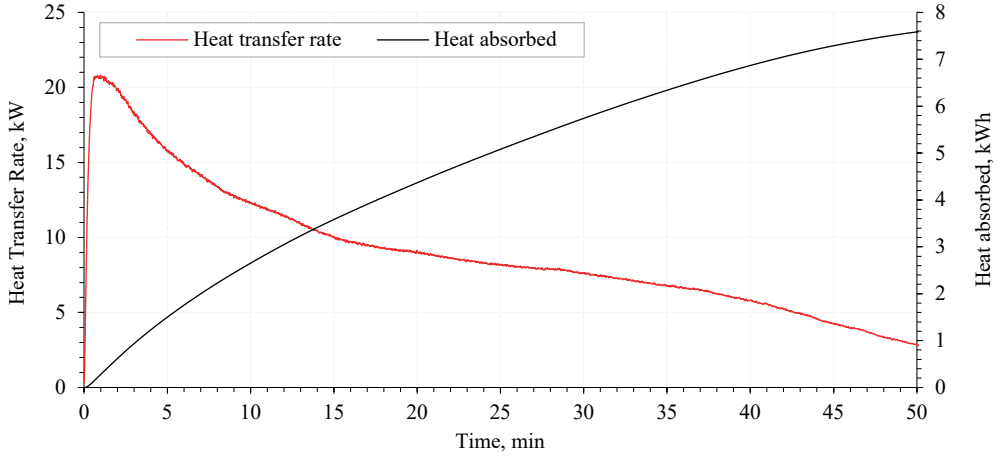

Fig. 4. Heat transfer rate and heat absorbed during the charging (melting) process.

3.2. PCM TES Discharging

The PCM TES discharging experiment (PCM solidification) showed the temperature variation of the HTF and PCM, the heat transfer rate of the HX, and the amount of heat released. The temperature distribution graph is presented in Fig. 5, while the heat transfer rate and energy curves for the entire discharging process are shown in Fig. 6.

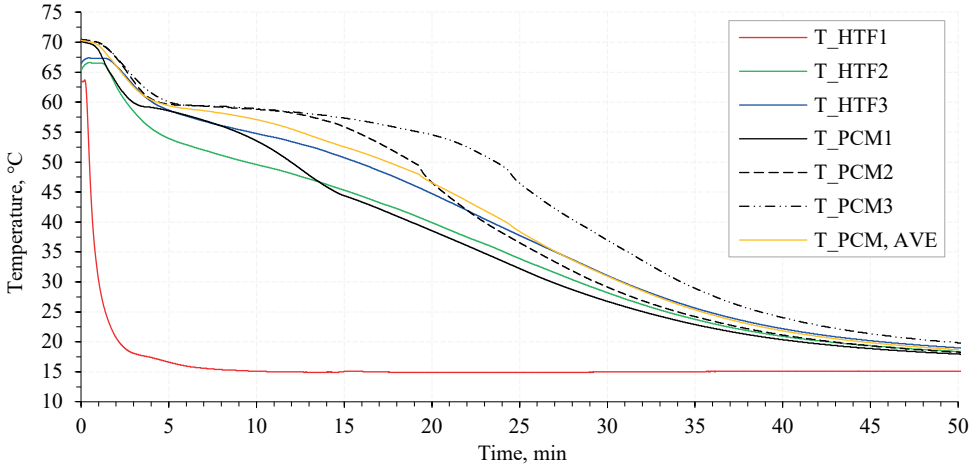

Fig. 5. Temperature distribution of HTF and PCM during the discharging (solidification) process.

From Fig. 5, it is observable that during the discharging experiment, the temperature of the PCM at the measurement locations T_{PCM1}, T_{PCM2}, and T_{PCM3} reaches the phase transition range of 59 °C after 4 min 10 s, 8 min 34 s, and 9 min 22 s, respectively. However, it should be noted that the slope of temperature curves decreases before the temperature reaches 59 °C, indicating that phase transition begins earlier (from 60 °C). The phase change process (solidification), until the temperature drops from 59 °C to 53 °C, takes 6 min 10 s for T_{PCM1}, 8 min 32 s for T_{PCM2}, and 12 min 17 s for T_{PCM3}. This shows that at the measurement point closer to the cold-water inlet (T_{PCM1}) the energy is released faster than at T_{PCM2} and T_{PCM3}. In

addition, the temperature difference at the beginning of the process, from 59.7 °C to 58.2 °C for the T_{PCM2}, and T_{PCM3}, is less than 0.2 °C, indicating similar PCM solidification characteristics in these areas of the HX. In terms of HTF temperature, a large temperature difference is observed (Fig. 5) between the inlet and outlet of HX. The temperature T_{HTF1} stabilises and reaches a set value of 15 °C after 10 min of the discharging process. For L1 (T_{HTF1} and T_{HTF2}), the maximum temperature difference of 42.1 °C is observed at 1 min 42s, and at the end of the process, ΔT decreases to 4.4 °C. The average ΔT of L1 during the entire process is 21.7 °C, which is 3.0 °C higher compared to the charging process. For L2 (T_{HTF2} and T_{HTF3}), the temperature difference is significantly lower compared to L1, reaching a maximum ΔT of 5.5 °C after 12 min 42 s from the beginning of the process. The average ΔT during the entire process is 3.5 °C, which is 1.3 °C higher compared to the charging process. The discharging process duration, until the average PCM temperature reaches 20 °C, is 44 minutes. The heat transfer rate during the discharging operation varies according to the temperature differential between HTF and PCM (Fig. 6).

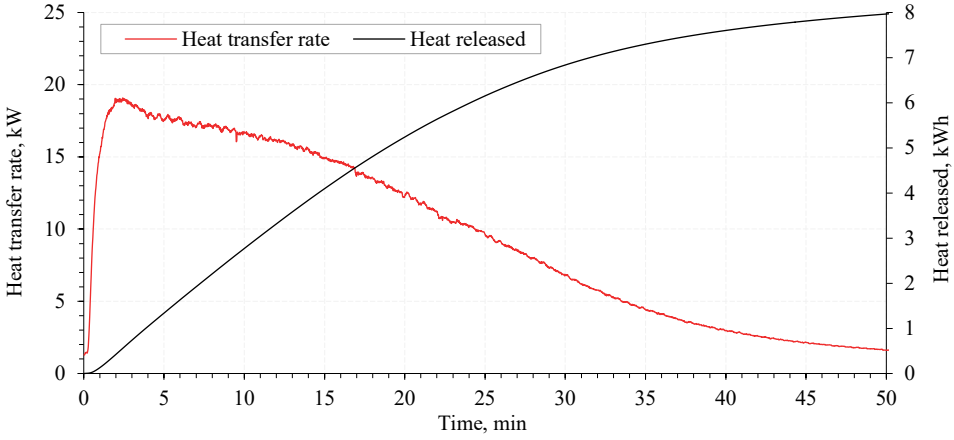

Fig. 6. Heat transfer rate and Heat released during the discharging (solidification) process.

Fig. 6 shows that the heat transfer rate reaches a maximum value of 19.2 kW at 1 min 58 s from the beginning of discharging and decreases to 2.2 kW when the average PCM temperature ($T_{PCM, AVE}$) reaches 20 °C after 44 minutes. The average heat transfer rate throughout the entire discharging process is 10.6 kW. This means that the maximum discharging power is 8.14 % lower than the charging power, and the discharging power at the end of the process is 35.3 % lower. However, the average discharging power is 14.0 % higher than the charging power. This higher average heat transfer rate is due to a larger average temperature difference between the HTF and the PCM during the discharging process. Compared to the charging process, a higher heat transfer rate is observed between 2 min 44 s and 28 min 15 s (Fig. 4 and Fig. 6). As a result, a larger amount of energy is released during this time interval, leading to a 10 min 11 s shorter overall discharging time compared to charging. It means that 7.48 kWh of energy is released in 37 min 49 s ($T_{PCM, AVE}$ is 23.1 °C). It should be noted that the discharging process took 44 minutes to reach an average PCM temperature of 20 °C. In this case, the amount of energy is 4.0 % (0.3 kWh) higher, indicating temperature gradient, thermal inertia in the PCM, and uneven distribution of the solid-liquid phase. To reduce the impact of this effect when determining the average temperature of PCM, a larger number of temperature sensors would be required, which is impractical in real-world applications.

4. CONCLUSION

An experimental investigation is presented to evaluate the thermal performance of PCM-based TES. To provide valuable insights into the design and operation of PCM TES, the analysis focuses on parameters such as HTF and PCM temperature, charging and discharging heat transfer rate and duration, and thermal energy stored and released.

This study shows that, in the series configuration of the HX, a higher temperature difference between the HTF inlet and outlet is observed in the first loop (L1) during both the charging and discharging processes. The PCM temperature distribution at different measuring points shows an uneven phase transition, caused by the low thermal conductivity of PCM and the decreasing HTF temperature difference across the HX.

The results demonstrate that the duration of the charging process, within the average PCM temperature range of 20–70 °C, is 48 minutes. The amount of heat stored is 7.48 kWh, and the average heat transfer rate is 9.3 kW. During the discharging process, 7.48 kWh of heat is released until the average PCM temperature reaches 23.1 °C. The average heat transfer rate during the entire discharging process is 14 % higher (10.6 kW) compared to charging, leading to a 10 min 11 s (21.2 %) shorter discharging time.

REFERENCES

[1] Rendall J., Elatar A., Nawaz K., Sun J. Medium-temperature phase change material integration in domestic heat pump water heaters for improved thermal energy storage. *Renewable and Sustainable Energy Reviews* 2023:185:113656. https://doi.org/10.1016/J.RSER.2023.113656

[2] Olympios A. V., Sapin P., Freeman J., Olkis C., Markides C. N. Operational optimisation of an air-source heat pump system with thermal energy storage for domestic applications. *Energy Conversion and Management* 2022:273:116426. https://doi.org/10.1016/J.ENCONMAN.2022.116426

[3] Douvi E., Pagkalos C., Dogkas G., Koukou M. K., Stathopoulos V. N., Caouris Y., Vrachopoulos M. G. Phase change materials in solar domestic hot water systems: A review. *International Journal of Thermofluids* 2021:10:100075. https://doi.org/10.1016/J.IJFT.2021.100075

[4] Javadi F. S., Metselaar H. S. C., Ganesan P. Performance improvement of solar thermal systems integrated with phase change materials (PCM), a review. *Solar Energy* 2020:206:330–352. https://doi.org/10.1016/J.SOLENER.2020.05.106

[5] Dzikevics M., Veidenbergs I., Valančius K. Sensitivity Analysis of Packed Bed Phase Change Material Thermal Storage for Domestic Solar Thermal System. *Environmental and Climate Technologies* 2020:24(1):378–391. https://doi.org/10.2478/rtuect-2020-0022

[6] Szajding A., Kuta M., Cebo-Rudnicka A., Rywotycki M. Analysis of work of a thermal energy storage with a phase change material (PCM) charged with electric heaters from a photovoltaic installation. *International Communications in Heat and Mass Transfer* 2023:140:106547. https://doi.org/10.1016/J.ICHEATMASSTRANSFER.2022.106547

[7] Royo P., Johnson M., David N., Fiss M., López-Sabirón A. M., Ferreira G. A., Gutierrez A. Experimental analysis of a power-to-heat storage with high-temperature phase change materials to increase flexibility and sector coupling. *Applied Thermal Engineering* 2024:236:121889. https://doi.org/10.1016/J.APPLTHERMALENG.2023.121889

[8] Resch A., Dehner H. Economic Analysis of Mobile Thermal Energy Storages as Complement to District Heating. *Environmental and Climate Technologies* 2023:27(1):516–531. https://doi.org/10.2478/rtuect-2023-0038

[9] Narbuts J., Vanaga R. Revolutionizing the Building Envelope: A Comprehensive Scientific Review of Innovative Technologies for Reduced Emissions. *Environmental and Climate Technologies* 2023:27(1):724–737. https://doi.org/10.2478/rtuect-2023-0053

[10] Narbuts J., Vanaga R. Nano-Enhanced Phase Change Materials for Building Envelopes: A Systematic Review of Thermal Performance and Applications. *Environmental and Climate Technologies* 2025:29(1):359–389. https://doi.org/10.2478/rtuect-2025-0025

[11] NematpourKeshteli A., Mahmoudi A., Iasiello M., Langella G., Bianco N. Experimental and numerical assessment of thermal characteristics of PCM in a U-shaped heat exchanger using porous metal foam and NanoPowder. *Solar Energy Materials and Solar Cells* 2024:274:112970. https://doi.org/10.1016/J.SOLMAT.2024.112970

[12] Kalapala L., Devanuri J. K. Influence of operational and design parameters on the performance of a PCM based heat exchanger for thermal energy storage – A review. *Journal of Energy Storage* 2018:20:497–519. https://doi.org/10.1016/J.EST.2018.10.024

[13] Choure B. K., Alam T., Kumar R. A review on heat transfer enhancement techniques for PCM based thermal energy storage system. *Journal of Energy Storage* 2023:72(A):108161. https://doi.org/10.1016/J.EST.2023.108161

[14] Abdellatif H. E., Belaadi A., Arshad A., Chai B. X., Ghernaout D. Enhancing thermal energy storage system efficiency: Geometric analysis of phase change material integrated wedge-shaped heat exchangers. *Applied Thermal Engineering* 2025:262:125268. https://doi.org/10.1016/J.APPLTHERMALENG.2024.125268

[15] Fadl M., Mahon D., Eames P. C. Thermal performance analysis of compact thermal energy storage unit-An experimental study. *International Journal of Heat and Mass Transfer* 2021:173:121262. https://doi.org/10.1016/J.IJHEATMASSTRANSFER.2021.121262

[16] Muraleedharan Nair A., Wilson C., Kamkari B., Locke J., Jun Huang M., Griffiths P., Hewitt N. J. Advancing Thermal Performance in PCM-Based Energy Storage: A Comparative Study with Fins, Expanded Graphite, and Combined Configurations. *Energy Conversion and Management*: *X* 2024:23:100627. https://doi.org/10.1016/J.ECMX.2024.100627

[17] Thonon M., Fraisse G., Zalewski L., Pailha M. Simultaneous charging and discharging processes in latent heat thermal energy storage: A review. *Thermal Science and Engineering Progress* 2024:47:102299. https://doi.org/10.1016/J.TSEP.2023.102299

[18] Herbinger F., Groulx D. Experimental comparative analysis of finned-tube PCM-heat exchangers' performance. *Applied Thermal Engineering* 2022:211:118532. https://doi.org/10.1016/J.APPLTHERMALENG.2022.118532

[19] Pakalka S., Valančius K., Streckienė G. Experimental comparison of the operation of PCM-based copper heat exchangers with different configurations. *Applied Thermal Engineering* 2020:172:115138. https://doi.org/10.1016/J.APPLTHERMALENG.2020.115138

[20] Pakalka S., Donėlienė J., Rudzikas M., Valančius K., Streckienė G. Development and experimental investigation of full-scale phase change material thermal energy storage prototype for domestic hot water applications. *Journal of Energy Storage* 2024:80:110283. https://doi.org/10.1016/j.est.2023.110283

[21] European Commission. EU regulation no 814/2013 implementing directive 2009/125/EC of the European Parliament and of the council with regard to ecodesign requirements for water heaters and hot water storage tanks. *Official Journal of European Union* 2013: L 346. http://data.europa.eu/eli/reg/2013/814/2017-01-09

[22] ISO 12241:2022. Thermal insulation for building equipment and industrial installations – Calculation rules. [Online]. [Accessed 10.06.2025]. Available: https://www.iso.org/standard/74655.html